A TWO-STAGE AUTOMATED FRAMEWORK FOR QUANTITATIVE MORPHOLOGICAL ANALYSIS OF MAST CELL DEGRANULATION IN HISTOPATHOLOGICAL IMAGES BASED ON YOLO AND CNN

Enna Chen¹, Jiadong Li¹, Xuan Qiao¹, Liujie Ren⁴, Zouqin Huang Mei Yao Yao Yi Yu $^{\boxtimes,1}$ and Yi Yu $^{\boxtimes,2}$

¹Shanghai Key Laboratory of Acupuncture Mechanism and Acupoint Function, School of Biomedical Engineering and Technology Innovation, Fudan University, Shanghai 200433, China, ²College of Medical Instruments, Shanghai University of Medicine & Health Sciences, Shanghai 201318, China, ³Shanghai Pudong New Area Traditional Chinese Medicine Hospital, Shanghai 200120, China, ⁴Eye and ENT Hospital of Fudan University, Shanghai 200031, China

e-mail: 24110290022@m.fudan.edu.cn, 20300290018@m.fudan.edu.cn, 25113060025@m.fudan.edu.cn, renliujie@fudan.edu.cn, hzqmusic@yeah.net, weiyao@fudan.edu.cn, 2200009@sumhs.edu.cn (Received November 12, 2025; accepted November 16, 2025)

ABSTRACT

Quantitative analysis of mast cell (MC) morphology and degranulation states is crucial for assessing inflammatory responses and therapeutic efficacy in biomedical research. This study presents a novel two-stage deep learning framework for the automated quantitative morphological analysis of MC degranulation states in toluidine blue-stained histological sections. We constructed a specialized dataset of 1,054 rat tissue images. In the detection stage, YOLOv11m achieved superior performance with a mean average precision (mAP@0.5) of 84% for locating MCs amidst complex tissue backgrounds. In the classification stage, using the model we previously acquired to extract pure mast cell images, EfficientNetV2-S attained an accuracy of 89.6% ± 2.1% in discriminating degranulation states through fine-grained morphological analysis. Critically, Class Activation Mapping (CAM) visualization demonstrated that the model's decision logic aligns precisely with pathological features of degranulation—such as membrane rupture and granule dispersal—thereby providing interpretable morphological evidence for automated classification. The proposed framework effectively decouples the tasks of cell localization and state classification, offering a robust, efficient, and morphologically interpretable solution for quantitative image analysis in histopathology. This approach has significant applications in acupuncture mechanism research and can be extended to other fields requiring granular structure analysis.

Keywords: Class Activation Mapping, CNN, Degranulation, Mast Cell, Quantitative Image Analysis, YOLO.

INTRODUCTION

Quantitative analysis of cell morphology in histopathological images is crucial for research in immunology and inflammation. Mast cells (MCs) are of particular interest due to their complex functional states (Austen and Boyce 2001), which are reflected in their morphological dynamics, especially degranulation (Krystel-Whittemore et al. 2016). Their granules—intact or released—directly indicate cellular activation and function (Ito et al. 2008). In tumors, mast cell density and location affect cancer progression; activated MCs also interact with immune or stromal cells to either modulate immunity or promote tumor growth (Guo et al. 2023). In inflammation, MCs serve as key effector cells through degranulation (Yang et al. 2023). Their roles in both contexts are closely tied to their activation state and spatial distribution (Vazquez et al. 2024; Wang et al. 2024; Johnson et al. 2017; Gaudenzio et al. 2016).

The quantification of MC counts and degranulation rates is a cornerstone of immunology and inflammation research, typically accomplished through microscopic analysis using staining techniques such as toluidine blue, followed by manual cell counting. In virology, influenza triggers mast cell (MC) recruitment to bronchial inflammation sites (Zarnegar et al. 2017); their degranulation is a key driver of excessive inflammation and tissue damage in SARS-CoV-2 infection (Cao et al. 2024). At injury sites, substance P release recruits MCs via Mrgprb2 (Albert-Bayo et al. 2019). While MCs can suppress inflammation in contact hypersensitivity (Reber et al. 2017), their degranulation is also targeted to alleviate inflammatory pain (Srebro et al. 2023). Pharmacologically, paeoniflorin alleviates urticaria by inhibiting MC degranulation (Wang et al. 2025). Notably, acupoints harbor denser MC populations; acupuncture prompts their accumulation and degranulation, releasing mediators

doi: 10.5566/ias.3751

that modulate local inflammation and function (Weber *et al.* 2001). Thus, MC recruitment, accumulation, and degranulation are central processes across these fields.

However, current manual counting methods present several notable drawbacks. First, they require substantial time and effort, often leading to issues such as repeated counting, omissions, or errors due to visual fatigue. Second, the identification of MC degranulation heavily relies on the individual experience of technicians, introducing significant subjectivity into the assessment. To manage the high resource demands of whole-slide analysis, researchers often adopt a field-of-view sampling strategy. Yet, since MCs frequently exhibit heterogeneous distribution within tissues (e.g., forming perivascular clusters), such sampling methods fail to adequately represent the entire tissue, inevitably introducing errors and compromising both data representativeness and statistical power.

Deep learning reliably supports interpretable decision-making in complex biomedical scenarios. Existing research demonstrates its strong capabilities in analyzing pathological images: for instance, a CNN model based on Inception v3 and PCA identifies fecal cellular images with 90.7% accuracy (Du *et al.* 2019). Notably, the YOLO series has advanced considerably in detecting diverse types of cells. One study integrated a FACE algorithm into YOLOv5 to improve yeast cell detection under difficult imaging conditions (Huang *et al.* 2023); another combined YOLO with deep active learning to enhance performance in detecting mitotic cells (Anaam *et al.* 2023). These findings confirm that improved YOLO architectures effectively handle complex biomedical image tasks.

Although deep learning has revolutionized cellular image analysis, current methods primarily detect and count common cell types like blood cells (Sun et al. 2025; Shi et al. 2024), tumor cells (Zhong et al. 2024; Haq et al. 2024), and germ cells (Kahveci et al. 2023; Wu et al. 2024), while automated approaches specifically designed to recognize mast cells and their degranulation states remain notably absent. Furthermore, stereological and morphometric methods (Gual-Vaya 2024), though computationally efficient and highly interpretable, adapt poorly to new devices or scenarios, generalize weakly, and struggle within complex cellular environments. Crucially, both paradigms largely overlook the challenge of automating fine-grained morphological classification to determine functional states—such as degranulation—in specialized cells like mast cells. Consequently, a significant gap exists in the development of automated frameworks dedicated to the morphometry of mast cell degranulation. This highly specialized cell type and its critical functional states remain excluded from mainstream computational pathology analysis.

We propose a novel two-stage deep learning framework for the quantitative analysis of mast cell degranulation states, integrating high-precision localization with fine-grained morphological classification. The first stage employs YOLO series models to rapidly locate cell regions and perform initial classification, while the second stage constructs dedicated CNN models to achieve detailed morphological classification of degranulation states. Most importantly, we incorporate Class Activation Mapping (CAM) to provide interpretable morphological insights, ensuring that model decisions align with pathological features.

MATERIALS AND METHODS

OVERALL RESEARCH FRAMEWORK

This study proposes a two-stage deep learning framework, as illustrated in Fig.1, which achieves precise identification of MCs and their degranulation states through the synergistic integration of object detection and fine-grained classification. In the first stage, YOLO series models are employed to localize and preliminarily classify MCs within the tissue images. The second stage involves constructing classification models based on transfer learning, utilizing deep neural networks such as ResNet101, ResNet152, ResNeXt-50, and EfficientNetV2-S to discriminate the degranulation states. The framework integrates strategies for data augmentation, class balancing, and model optimization, significantly enhancing detection efficiency and classification robustness.

MAST CELL DATASET DESCRIPTION

MC Detection Dataset

Due to the absence of public standard datasets for mast cell pathology slides, this study leveraged samples from acupuncture interventions at rat Zusanli (ST36) points accumulated by our laboratory and collaborators between 2023-2025. All animal procedures were performed in strict compliance with internationally recognized ethical standards for laboratory animal care and use, and were formally approved by the Institutional Animal Care and Use Committee (IACUC) of Shanghai University of Traditional Chinese Medicine (Approval No. PZSHUTCM2308010011). Rat tissue sections stained with toluidine blue exhibit purple coloration through specific heparin granule-dye binding, enabling direct observation of MC granule morphology and

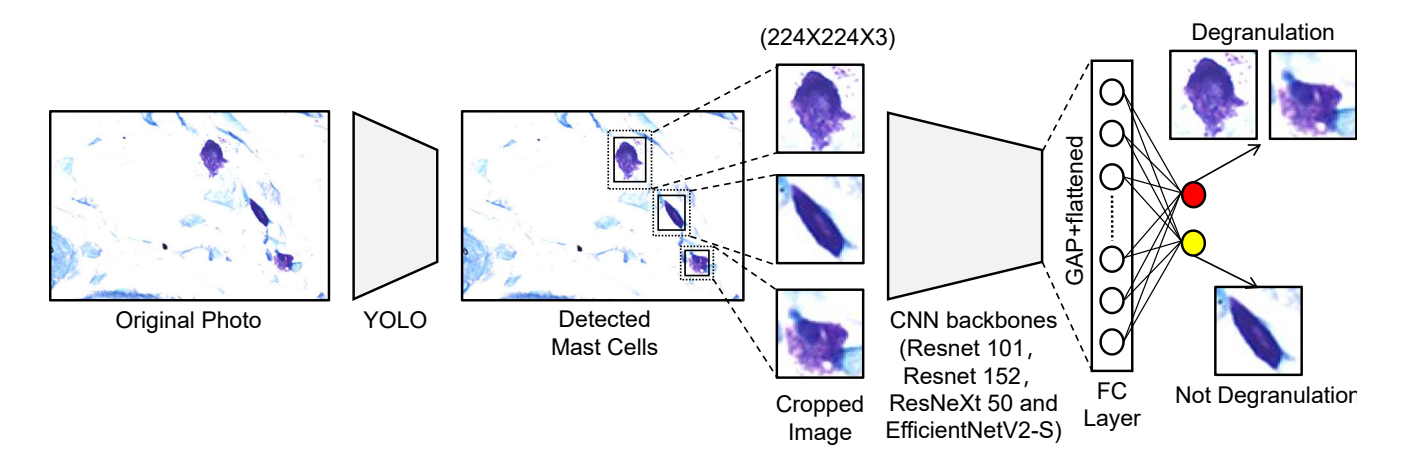


Fig. 1. Framework for mast cell identification and fine-grained classification. Mast cell regions are localized and cropped via You Only Look Once detection, followed by fine-grained classification of degranulated versus non-degranulated states using a convolutional neural network-based model.

degranulation states (Reber *et al.* 2017; Klatt *et al.* 1983). The staining process yielded 1,054 rat mast cell slide images captured at 400× magnification using an optical microscope (NTB900-FL, Ningbo Yongxin Optical, China) and an inverted research microscope (Eclipse Ti-S; Nikon, Japan), with digital images acquired through an MShot MSX2 camera controlled by MShot Image Analysis System V1.1.6 software.

This dataset was rigorously annotated through a manual process: Researcher A initially labeled all mast cell bounding boxes (for localization only) using LabelImg. Subsequently, Researchers B and C independently and blindly assessed each cell, assigning binary classification labels (0 = non-degranulated, 1 = degranulated). Finally, samples with inconsistent classifications were subjected to a joint review by B and C to determine the final judgment.

The morphological identification criteria for MCs degranulation are primarily based on the following three characteristic changes; the presence of any one indicator qualifies the cell as degranulated: First, cytoplasmic granules penetrate the plasma membrane and distribute in the peripheral region of the cell; Second, the cell margin exhibits an irregular morphology, with a significantly increased perimeter and blurred boundary; Third, toluidine blue staining reveals abnormal vacuolar structures within the cytoplasm exceeding twice the diameter of normal granules. Non-degranulated MCs exhibit a typical morphology with a complete shape and smooth, clearly defined boundaries. Representative figures are shown in Supplementary Material, Fig.S1(left vs. right, ND vs. D).

MC Classification Dataset

Based on the optimal YOLO MC detection model identified during initial training (with an input resolution of 640×640 and a confidence threshold of 0.5), cells were located within the whole-slide images and subsequently cropped to obtain pure-region image samples. The degranulation labels for these cropped images originate directly from the final gold standard dataset described in the "MC Detection Dataset" section—labels that researcher B and C agreed upon after joint review. Their task involved verifying and confirming that each cropped cell image correctly corresponded to its label in the gold standard set, ensuring no image-label mismatch occurred during dataset construction. This quality control process guarantees the reliability of the dataset used to evaluate subsequent classification models.

MAST CELL DETECTION BASED ON YOLO MODELS

This study employs YOLOv5 and YOLOv11 the foundational detection frameworks. The YOLO series algorithms are renowned for their real-time efficient detection capabilities and balanced accuracy-speed performance, making them suitable for the rapid localization of dense, small targets like mast cells. For YOLOv5, we implemented Ultralytics adopted the officially models YOLOv5n, YOLOv5s, and YOLOv5m; For YOLOv11, we used the models provided in Ultralytics YOLO: YOLOv11n, YOLOv11m, YOLOv11l, and YOLOv11x (code repository: https://github. com/ultralytics). Mast cell slice images were divided into training and validation sets in a 7:3 ratio. Input images were uniformly resized to 640×640 pixels, and the training batch size was set to 16. Extended methodological specifications appear in Supplementary Sections S1.1.

CNN-BASED MAST CELL CLASSIFICA-TION

To balance model depth and computational efficiency, this study selected ResNet-101, ResNet-152, ResNeXt-50, and EfficientNetV2-S as multiscale feature extractors. All models were trained and evaluated using a rigorous 10-fold cross-validation strategy. During transfer learning, we adopted a layerwise unfreezing strategy, progressively unlocking convolutional layers combined with adaptive learning rate scheduling. For the binary classification task distinguishing degranulated versus non-degranulated mast cells, a newly constructed classification head with a single output neuron (Sigmoid activation) was fine-tuned. This transfer learning strategy effectively mitigated medical image data scarcity. Extended methodological specifications appear in Supplementary Sections S1.2.

PERFORMANCE EVALUATION STRAT-EGY

This study employed the confusion matrix, Area Under the Curve (AUC), and mean Average Precision (mAP) as core evaluation metrics. Classification results were visualized via heatmaps generated with the Seaborn library, using color gradients and numerical annotations to illustrate outcome distributions. The confusion matrix summarized model performance by tabulating True Positives (TP), True Negatives (TN), False Positives (FP), and False Negatives (FN). Based on these values, Precision, Recall, Accuracy, and the F1 score were computed to further assess classification efficacy.

Detailed calculation formulas for each metric are provided in the following section:

$$Precision = \frac{TP}{(TP + FP)},$$
 (1)

$$Accuracy = \frac{(TP + TN)}{(TP + TN + FP + FN)},$$
 (2)

$$Recall = \frac{TP}{(TP + FN)},$$
 (3)

$$F1 = 2 \cdot \frac{\text{Precision} \cdot \text{Recall}}{\text{Precision} + \text{Recall}},$$
 (4)

Precision (Eq.1) measures the proportion of true degranulated samples among those predicted as

degranulated. Accuracy (Eq.2) evaluates the overall predictive performance by calculating the ratio of correctly predicted samples to the total. Recall (Eq.3) reflects the model's ability to identify actual degranulated samples. The F1-score (Eq.4), as the harmonic mean of Precision and Recall, balances both metrics and is particularly informative in classimbalanced scenarios. AUC defined in Eq.(5):

$$AUC = \frac{1}{M \cdot N} \sum_{i=1}^{M} \sum_{j=1}^{N} \left[I\left(f(x_i^+) > f(x_j^-)\right) + 0.5 \cdot I\left(f(x_i^+) = f(x_j^-)\right) \right],$$
(5)

measures the model's ability to discriminate between positive (degranulated) and negative (non-degranulated) mast cells. It represents the probability that a randomly chosen positive instance receives a higher prediction score than a negative one across all thresholds. As a threshold-independent metric, AUC robustly evaluates global ranking performance and remains unaffected by class imbalance, which is common in histopathological image analysis. To address the requirements for mast cell localization and confidence estimation, the mean Average Precision (the mAP) metric is introduced as defined in Eq.(6):

$$mAP = \frac{\sum_{i=1}^{N} A \cdot P_i}{N} = \frac{\sum_{i=1}^{N} \int_0^1 P_i(R_i) dR_i}{N}, \quad (6)$$

where N denotes the number of classes (binary classification in this study) and AP_i represents the Average Precision for class i. This metric comprehensively quantifies the model's robust recognition capability for degranulation events in mast cell histology images by integrating the precision-recall trade-off across multiple confidence thresholds.

RESULTS

DEFINITIVE GROUND TRUTH ESTAB-LISHMENT FOR MC DETECTION AND DEGRANULATION ASSESSMENT

Researcher A annotated 1,054 rat mast cell histology images and identified 2,325 mast cells. This study employed a blinded design where two independent researchers (B and C) classified degranulation states across all 2,325 purified mast cell samples. Their consensus outcomes appear in Table 1. The calculated Kappa coefficient ($\kappa = 0.78$, p < 0.001) demonstrates statistically significant high inter-observer agreement.

Table 1. Manual Verification Results of Mast Cell Degranulation State Based on MC Detection Dataset

Manual Verification	Degranulated (Positive)	Non-Degranulated (Negative)	Total-B
Degranulated (Positive)	1648	13	1661
Non-Degranulated (Negative)	176	488	664
Total-C	1824	501	2325

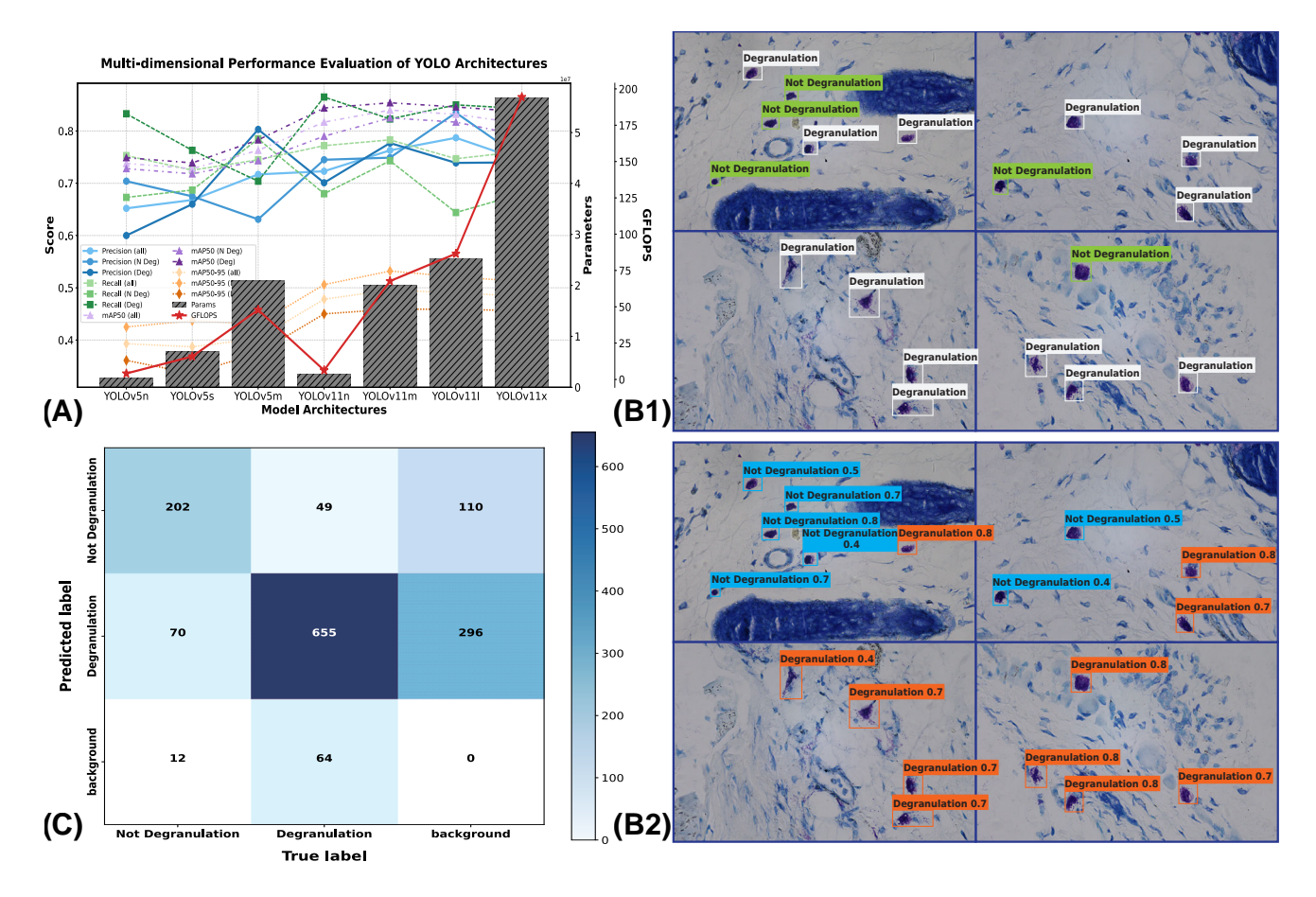


Fig. 2. Performance evaluation of mast cell recognition models. (A) Multidimensional performance analysis of mast cell recognition models. All denotes overall performance, N Deg indicates non-degranulated mast cells, and Deg represents degranulated mast cells. (B) Detection results of mast cells and their degranulation states by the YOLOv11m model; Subfigure (B1) visualizes ground truth bounding boxes, while (B2) displays predicted bounding boxes with confidence scores. (C) Confusion matrix for classification of mast cells and degranulation states using the YOLOv11m model.

Both researchers then jointly re-examined discordantly classified mast cells and established the definitive ground truth dataset. Technicians B and C achieved 95.27% and 95.18% classification accuracy respectively (Table S2). Their assessments closely aligned with the ground truth, both exceeding 95% accuracy.

OVERALL ASSESSMENT OF THE MAST CELL DETECTION MODEL

This study used seven model types: YOLOv5n, YOLOv5s, YOLOv5m, YOLOv11n, YOLOv11m, YOLOv11l, and YOLOv11x for mast cell detection training. Fig.2A shows the training results, and Table S1 in the Supplementary Sections provides specific numerical values.

As shown in Fig.2A and Table S1, the YOLOv11m model achieves an mAP50-all score of 0.84, significantly outperforming all YOLOv5 series models. It also attains a Recall-all score of 0.783, demonstrating comprehensive superiority over the YOLOv5 baselines (YOLOv5m: 0.745; YOLOv5s: 0.725; YOLOv5n: 0.753). These results indicate that its architectural optimizations simultaneously enhance both detection accuracy and target sensitivity.

The models show notable differences in recognizing degranulated versus non-degranulated mast cells, with generally better detection of degranulated cells. YOLOv11n achieves the highest recall for degranulated cells (0.865), but has significantly lower recall for non-degranulated cells (0.680), which may limit its generalization in mixed samples. For balanced performance, YOLOv11m is optimal, leading in mAP50 for degranulated cells (0.850) and showing competitive recall for non-degranulated cells (0.785), making it the most robust choice for comprehensive mast cell analysis.

YOLOv11m Model Results

Fig.2B compares the detection results of the YOLOv11m model against ground truth labels, showing accurate localization and classification of mast cell degranulation states based on morphological features. However, the model struggles to distinguish degranulation in dense cell regions with stromal interference, indicating limited robustness under complex histological noise. As shown in the confusion matrix in Figure 2C, the model achieves recall rates of 0.85 and 0.71 for degranulated and non-degranulated mast cells, respectively. Error analysis reveals that 296 and 110 background regions were misclassified as degranulated and non-degranulated cells, far exceeding the number of missed true cells

(64 degranulated and 12 non-degranulated). This indicates two main issues: first, overdiagnosis risk is higher than missed detection due to difficulty in distinguishing degranulated cells from complex stromal structures; second, the recognition capability for non-degranulated cells remains insufficient, limiting practical application. Further analyses are provided in Supplementary Material Fig.S2.

DEGRANULATION STATE CLASSIFICA-TION MODEL PERFORMANCE

Analysis of the previously trained YOLO model reveals that the optimal YOLOv11m model demonstrates certain errors in detecting degranulation states of mast cells and exhibits noticeable background misidentification. Therefore, we implement a CNN model to specifically identify mast cell degranulation, thus enhancing the overall accuracy of the model.

Fine-Grained Mast Cell Classification Results

To eliminate interference from the tissue microenvironment, this study employed a purified mast cell dataset (containing degranulated and non-degranulated samples), which was extracted using YOLOv11m and rigorously validated through manual verification. Using a transfer learning approach, ImageNetpretrained ResNet101, ResNet152, ResNeXt-50, and EfficientNetV2-S were selected as backbone models. Feature transfer was facilitated through layer-wise unfreezing and adaptive learning rate scheduling. Evaluation based on key classification metrics revealed significant differences in model performance regarding degranulation state recognition within the transfer learning framework (Zhu et al. 2024). The dynamic changes in training loss and validation accuracy throughout the 10-fold cross-validation are provided in Supplementary Material Fig. S3.

Experimental results (Fig.3A) show that the EfficientNetV2-S model achieved the best overall performance in cross-validation. It attained a mean classification accuracy of 89.6% ± 2.1%, significantly outperforming ResNeXt-50 (85.0% ± 2.0%), ResNet101 (86.0% \pm 3.0%), and ResNet152 (86.0%) ± 2.0%). EfficientNetV2-S consistently outperformed other models in fine-grained classification, achieving a precision of 86.7% (±2.9%), a recall of 85.4% $(\pm 3.2\%)$, and an F1-score of 85.9% $(\pm 2.9\%)$. It surpassed the second-best model (ResNet152) by margins of 3.1% in precision, 6.2% in recall, and 5.8% in F1-score. These results demonstrate EfficientNetV2-S effectively captures fine-grained features across mast cell subclasses, providing a robust solution for degranulation classification.

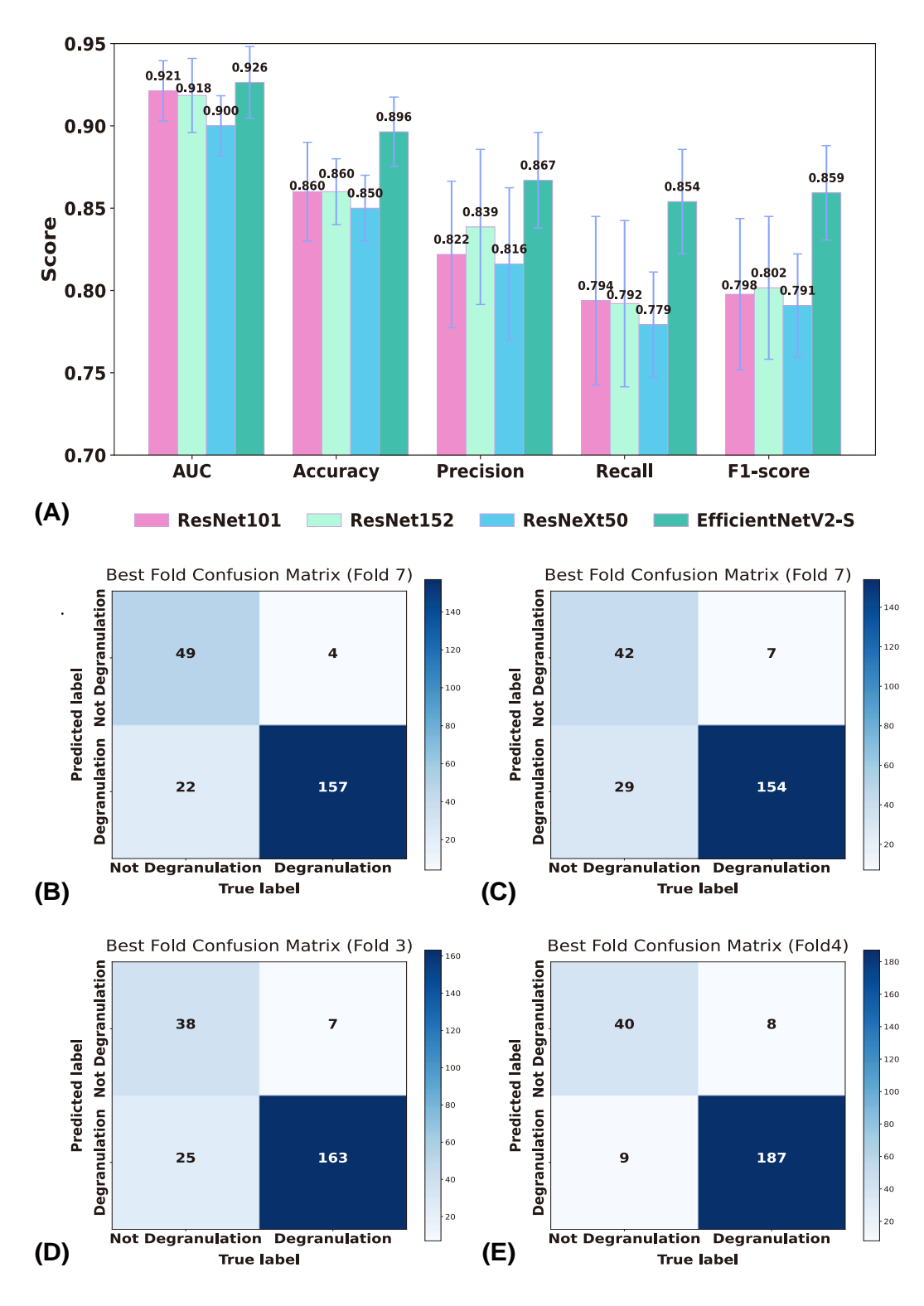


Fig. 3. Comprehensive Evaluation of Fine-Grained Mast Cell Degranulation Classifiers. (A) Overall performance metrics for mast cell degranulation state classification models; (B) Confusion matrix: Optimal ResNet101 classifier; (C) Confusion matrix: Optimal ResNet152 classifier; (D) Confusion matrix: Optimal ResNeXt-50 classifier; (E) Confusion matrix: Optimal EfficientNetV2-S classifier.

The current top-performing model, EfficientNetV2-S, achieves an average accuracy of 89.6% and a best accuracy of 92.7%, approaching the human classification benchmark of 95.27%. This finding demonstrates that lightweight models optimized via compound scaling may outperform complex architectures for fine-grained classification tasks. Its built-in SE (Squeeze-and-Excitation) attention mechanism (Hu *et al.* 2018) enhances the model's focus on degranulation-related features, such as membrane rupture and granule dispersion, by dynamically recalibrating channel-wise feature responses, while effectively suppressing interference from interstitial backgrounds.

Confusion Matrix Analysis

As shown in Fig.3(panels B-E) all four models identify degranulated mast cells more accurately than non-degranulated types due to class imbalance (degranulated samples triple non-degranulated). ResNeXt-50 achieved high sensitivity to degranulated cells but produced a false positive rate of 39.68% - 2.16 times that of EfficientNetV2-S (18.37%) - while both models maintained similar false negative rates (approximately 4.1%). EfficientNetV2-S limited false positives to only 9 cases and demonstrated high classification stability. These results identify EfficientNetV2-S as the optimal model, combining efficiency and balanced performance in complex, noisy medical imaging scenarios with pronounced class imbalance.

Feature Visualization

Employing CAM, we visualize model decision logic by reconstructing feature activation maps into 50×50 resolution space via bilinear interpolation and quantifying activation intensity with Jet colormap. Analysis reveals divergent attention mechanisms across models for mast cell degranulation assessment (Fig.S4).

As shown in Fig.S4, distinct activation patterns were observed across models for non-degranulated samples. ResNet101 exhibited radially expanding activation from the nuclear region, ResNet152 showed synchronized activation at dual cross-membrane interfaces, and ResNeXt-50 displayed pronounced extracellular matrix-oriented activation. In contrast, EfficientNetV2-S consistently localized activations to perinuclear dense areas and membrane edges, effectively minimizing interference from transmembrane noise.

For degranulated samples, all four models concentrate attention on granule dispersal areas, aligning with clinical "granule exocytosis" patterns, yet diverge in granularity: ResNeXt-50/ResNet models overemphasize discrete granule boundaries and overweight stromal context, while EfficientNetV2-S activates regionally diffuse areas covering both the cell body and dispersed granules—demonstrating strong consistency with manual classification standards. The corresponding CAM visualizations are presented in Fig.4.

DISCUSSION

DETECTION MODEL PERFORMANCE ANALYSIS

The YOLOv11 architecture, enhanced with spatial attention and dynamic label assignment (Khanam and Hussain 2024), is well-suited for mast cell detection in histopathological images. In dense tissue regions, YOLOv11m achieved a higher mAP@50 than YOLOv5m (0.84 vs. 0.76) with a comparable parameter count, demonstrating superior architectural efficiency. Its effectiveness has also been supported in complex cellular environments such as dense blood cells (Sazak and Kotan 2025) and overlapping cervical cells (Wu *et al.* 2023). Nevertheless, YOLOv11m still exhibits clear limitations in distinguishing mast cell degranulation states.

These limitations underscore the necessity of our two-stage framework. Specifically, YOLOv11m shows a notable disparity in recall between degranulated and non-degranulated mast cells (0.823 vs. 0.743), reflecting the fundamental challenge detection models face in discriminating subtle inter-class morphological variations. While highly capable in localization, such models struggle with fine-grained classification that requires distinguishing degranulation patterns from complex background noise. To address this, we introduced a dedicated CNN classifier for detailed image analysis. This two-stage approach leverages YOLO's high-sensitivity candidate detection, followed by CNN-based re-evaluation of each cell's state. As a result, the false positive rate for degranulation recognition decreased from 25.74% to 18.37%, confirming the critical role of the dedicated classification stage in improving the accuracy of mast cell state analysis in histopathological images.

PERFORMANCE DISPARITY ANALYSIS OF CLASSIFICATION MODELS

Performance disparities among the four finegrained mast cell classifiers arise from inherent architectural differences. ResNet architectures exhibit

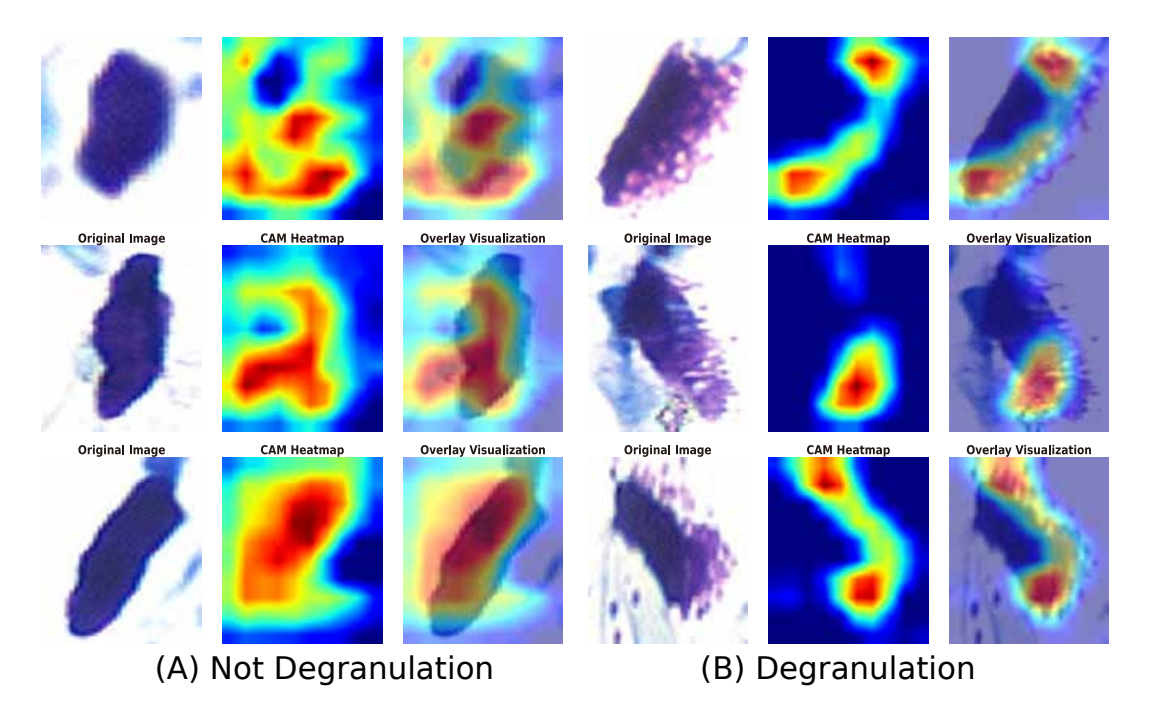


Fig. 4. Visualization of CAM using the optimal EfficientNetV2-S framework. (A) Not Degranulation category displays original images, CAM heatmaps, and activation maps for three representative cases. (B) Degranulation category presents corresponding image sets for three samples.

oversensitivity to local textures due to gradient propagation constraints. Studies show that when physical depth (d) far exceeds effective gradient depth (1), residual units degrade into static processors (Wu et al. 2019), and uniform scaling amplifies redundancy, emphasizing local noise over semantic context (Lin et al. 2023). This leads to: (1) inadequate low-level feature extraction with noise sensitivity, and (2) overreliance on high-level static features, exaggerating local patterns like granule boundaries. While ResNeXt-50 improves local feature reuse via group convolutions, it fails to address core deep network issues. In contrast, EfficientNetV2-S employs compound scaling and dynamic training for efficient feature extraction and noise suppression (Tan and Le 2021), reducing false positives to only 9 cases (Fig.3E)—consistent with Abd El-Aziz et al. (2025)'s leukemia classification results. The integrated SE attention mechanism, combined with CAM visualization, further validates the model's biologically relevant decision-making (Fig. 4), helping to bridge the gap between deep learning's 'black box' nature and interpretable morphological analysis.

PRACTICAL APPLICATIONS

This study presents a two-stage deep learning framework with broad pathological applicability. By automating the recognition of mast cell degranulation, the system reduces manual analysis time from hours to minutes per batch, greatly accelerating quantitative assessment in areas such as infectious disease, tissue damage, inflammation, drug studies, and acupuncture research. Its in situ detection capability without requiring segmentation offers a new paradigm for examining mast cell dynamics within tissue microenvironments and bridges a critical gap in functional cell state identification. The framework supports an AI-assisted workflow that integrates fully automated screening with human-AI collaboration: the YOLO-EfficientNet model conducts panoramic scanning and initial detection of tissue sections, automatically accepts high-confidence degranulation predictions (≥ 0.7) , and produces digital pathology reports including spatial coordinates, classification states, and confidence scores. Detections below the confidence threshold trigger expert review, with priority given to verifying "non-degranulated" classifications.

LIMITATIONS AND FUTURE WORK

This study has three primary limitations: First, dataset constraints pose challenges to model generalization, though our pipeline demonstrated robust feasibility for the target task. Second, distinct model architectures exhibit significant performance divergence in specific detection scenarios—YOLOv11m excels at detecting degranulated mast cells while YOLOv11l shows superior performance for non-degranulated cells—highlighting the framework's

need for improved adaptability to cellular phenotypic diversity. Furthermore, addressing false positives in complex tissue backgrounds requires refining feature learning mechanisms.

Future work will address these challenges through two key initiatives: First, expanding mast cell data diversity in subsequent experiments while leveraging generative AI (e.g., GANs and DDIM) to synthesize non-degranulated cell samples—creating balanced training sets. Second, deploying the algorithm onto digital pathology scanners to develop clinical modules supporting real-time microscopic imaging analysis, enabling dynamic monitoring of mast cell responses during acupuncture interventions.

CONCLUSIONS

This study presents an interpretable deep learning framework for high-throughput analysis of mast cell degranulation. Using a dedicated dataset of 1,054 annotated images, our two-stage system combines YOLOv11m for efficient cell detection (0.84 mAP@50) and EfficientNetV2-S for fine-grained morphological classification (89.6% mean accuracy and 92.7% peak accuracy). CAM ensures pathological interpretability by highlighting discriminative features. This approach enables robust analysis of cellular dynamics in tissue microenvironments, with applications in acupuncture mechanism research and inflammatory diseases.

ACKNOWLEDGEMENT

This research was funded by the National Key R&D Program of China (2024YFC3505200 (Yao) and 2024YFC3505202 (Yao)), the National Natural Science Foundation of China, grant number 12172092 (Yao), 82305416 (Yu), 82174488 (Yao). New Quality Clinical Specialty Program of High-end Medical Disciplinary Construction in Shanghai Pudong New Area (2025-PWXZ-17) (Huang), Famous Traditional Chinese Medicine Studio Construction Project of Shanghai Pudong New Area Health Commission (PDZY-2025-0707) (Huang).

REFERENCES

Abd El-Aziz AA, Mahmood MA, Abd El-Ghany S (2025). A robust EfficientNetV2-s classifier for predicting acute lymphoblastic leukemia based on cross validation. Symmetry Basel 17:24.

- Albert-Bayo M, Paracuellos I, Gonzalez-Castro AM, Rodriguez-Urrutia A, Rodriguez-Lagunas MJ, Alonso-Cotoner C, Santos J, Vicario M (2019). Intestinal mucosal mast cells: Key modulators of barrier function and homeostasis. Cells 8:135.
- Anaam A, Al-antari MA, Hussain J, Samee NA, Alabdulhafith M, Gofuku A (2023). Deep active learning for automatic mitotic cell detection on HEp-2 specimen medical images. Diagnostics 13:1416.
- Austen KF, Boyce JA (2001). Mast cell lineage development and phenotypic regulation. Leuk Res 25:511–8.
- Cao JB, Zhu ST, Huang XS, Wang XY, Wu ML, Li X, Liu FL, Chen L, Zheng YT, Wang JH (2024). Mast cell degranulation-triggered by SARS-CoV-2 induces tracheal-bronchial epithelial in fl ammation and injury. Virol Sin 39:309–18.
- Du X, Liu L, Wang X, Ni G, Zhang J, Hao R, Liu J, Liu Y (2019). Automatic classification of cells in microscopic fecal images using convolutional neural networks. Biosci Rep 39:BSR20182100.
- Gaudenzio N, Sibilano R, Marichal T, Starkl P, Reber LL, Cenac N, McNeil BD, Dong X, Hernandez JD, Sagi-Eisenberg R, Hammel I, Roers A, Valitutti S, Tsai M, Espinosa E, Galli SJ (2016). Different activation signals induce distinct mast cell degranulation strategies. J Clin Invest 126:3981–98.
- Gual-Vaya L (2024). Classification of red blood cells from a geometric morphometric study. Image Anal Stereol 43:109–19.
- Guo X, Sun M, Yang P, Meng X, Liu R (2023). Role of mast cells activation in the tumor immune microenvironment and immunotherapy of cancers. Eur J Pharmacol 960:176103.
- Haq I, Mazhar T, Asif RN, Ghadi YY, Ullah N, Khan MA, Al-Rasheed A (2024). YOLO and residual network for colorectal cancer cell detection and counting. Heliyon 10:e24403.
- Hu J, Shen L, Albanie S, Sun G, Wu E (2018). Squeeze-and-excitation networks. In: IEEE Conference on Computer Vision and Pattern Recognition (CVPR), vol. /.
- Huang ZJ, Patel B, Lu WH, Yang TY, Tung WC, Bucinskas V, Greitans M, Wu YW, Lin PT (2023). Yeast cell detection using fuzzy automatic contrast enhancement (FACE) and you only look once (YOLO). Sci Rep 13:16222.
- Ito A, Hagiyama M, Oonuma J (2008). Nervemast cell and smooth muscle-mast cell interaction mediated by cell adhesion molecule-1, CADM1. J Smooth Muscle Res 44:83–93.

- Johnson MM, Mendoza R, Raghavendra AJ, Podila R, Brown JM (2017). Contribution of engineered nanomaterials physicochemical properties to mast cell degranulation. Sci Rep 7:43570.
- Kahveci B, Onen S, Akal F, Korkusuz P (2023). Detection of spermatogonial stem/progenitor cells in prepubertal mouse testis with deep learning. J Assist Reprod Genet 40:1187–95.
- Khanam R, Hussain M (2024). YOLOv11: An overview of the key architectural enhancements. arXiv preprint abs/2410.17725:/.
- Klatt EC, Lukes RJ, Meyer PR (1983). Benign and malignant mast-cell proliferations diagnosis and separation using a ph-dependent toluidine blue stain in tissue section. Cancer 51:1119–24.
- Krystel-Whittemore M, Dileepan KN, Wood JG (2016). Mast cell: A multi-functional master cell. Front Immunol 6:620.
- Lin C, Yang P, Wang Q, Qiu Z, Lv W, Wang Z (2023). Efficient and accurate compound scaling for convolutional neural networks. Neural Netw 167:787–97.
- Reber LL, Sibilano R, Starkl P, Roers A, Grimbaldeston MA, Tsai M, Gaudenzio N, Galli SJ (2017). Imaging protective mast cells in living mice during severe contact hypersensitivity. JCI Insight 2:e92900.
- Sazak H, Kotan M (2025). Automated blood cell detection and classification in microscopic images using YOLOv11 and optimized weights. Diagnostics 15:22.
- Shi CY, Zhu DL, Zhou CJ, Cheng S, Zou CY (2024). Gpmb-yolo: a lightweight model for efficient blood cell detection in medical imaging. Health Inf Sci Syst 12:24.
- Srebro D, Dozic B, Vuckovic S, Vujovic KS, Brkic BM, Dozic I, Srebro M (2023). The interactions of magnesium sulfate and cromoglycate in a rat model of orofacial pain; the role of magnesium on mast cell degranulation in neuroinflammation. Int J Mol Sci 24:6241.
- Sun H, Wan XR, Tang SG, Li YN (2025). SSW-YOLO: Enhanced blood cell detection with improved feature extraction and multi-scale attention. J Imaging Inform Med /:01460–3.
- Tan M, Le QV (2021). EfficientNetV2: Smaller models and faster training. In: International Conference on Machine Learning (ICML), vol. 139 of *Proceedings of Machine Learning Research*.

- Vazquez TAS, Lopez NL, Carmona MCS (2024). MASTer cell: chief immune modulator and inductor of antimicrobial immune response. Front Immunol 15:1360296.
- Wang X, Chen A, Pang Y, Hou C, Wang Y, Liu E, Zhao Y, Guo J, Li M (2025). Paeoniflorin as a potential agent for urticaria treatment: Suppressing mast cell degranulation through HMGB1/TLR4/NF-b signaling inhibition. Mol Immunol 183:33–43.
- Wang YX, Liu YH, Zhang ZL, Qiao X, Li YC, Ren LJ, Ding GH, Yao W, Yu Y (2024). Influence of acupuncture intensity on analgesic effects in AA rat models. Front Bioeng Biotechnol 12:1502535.
- Weber A, Knop J, Maurer M (2001). Pattern recognition analysis of human cutaneous mast cell populations by topographical total body surface mapping. J Invest Dermatol 117:791–.
- Wu J, Sun Y, Jiang Y, Bu Y, Chen C, Li J, Li L, Chen W, Cheng K, Xu J (2024). An automatic classification method of testicular histopathology based on SC-YOLO framework. Biotechniques 76:443–52.
- Wu NK, Jia DY, Zhang CW, Li ZQ (2023). Cervical cell extraction network based on optimized yolo. Math Biosci Eng 20:2364–81.
- Wu Z, Shen C, van den Hengel A (2019). Wider or deeper: Revisiting the ResNet model for visual recognition. Pattern Recognit 90:119–33.
- Yang BG, Kim AR, Lee D, An SB, Shim YA, Jang MH (2023). Degranulation of mast cells as a target for drug development. Cells 12:1506.
- Zarnegar B, Mendez-Enriquez E, Westin A, Söderberg C, Dahlin JS, Grönvik KO, Hallgren J (2017). Influenza infection in mice induces accumulation of lung mast cells through the recruitment and maturation of mast cell progenitors. Front Immunol 8:310.
- Zhong Z, Hou J, Yao Z, Dong L, Liu F, Yue J, Wu T, Zheng J, Ouyang G, Yang C, Song J (2024). Domain generalization enables general cancer cell annotation in single-cell and spatial transcriptomics. Nat Commun 15:1929.
- Zhu MY, Yang P, Bian C, Zuo FF, Guo ZM, Wang YF, Wang YJ, Bai YX, Zhang N (2024). Convolutional neural network-assisted diagnosis of midpalatal suture maturation stage in cone-beam computed tomography. J Dent 141:104808.